

The Measurement of Total Inclusion Content in Nickel-Titanium Alloys

Frank Sczerzenie, Giorgio Vergani, and Clarence Belden

(Submitted May 22, 2012; in revised form August 23, 2012)

Inclusion content is important for the properties of high performance alloys used in fatigue rated devices. A method to analyze the total inclusion content of NiTi alloys was applied to vacuum induction melted vacuum arc remelted hot rolled coil and cold drawn wire. Carbides and oxides populations were analyzed separately. Pursuant to ASTM standards, a definition for stringers was formulated and applied to cold drawn wire. It was shown that changes in melting and hot working result in changes in the amount and size of carbides and oxide inclusions. The inclusion size distributions are highly skewed. It is hypothesized that the statistics of extreme values must be applied to these populations in order to predict a maximum inclusion size.

Keywords advanced characterization, biomaterials, metallography, non-ferrous metals, optical microscopy, rolling

1. Introduction

Inclusion content is important for the properties of high performance alloys used in fatigue rated devices. Alloys such as NiTi and CoNiCrMo used in medical devices benefit from low inclusion content. As reported by Bradley for MP35N, improved microcleanliness increased fatigue life by 797% at a stress level of 689.5 MPa (Ref 1).

Inclusions may be categorized as exogenous or indigenous. Exogenous inclusions are from outside of the alloy such as pieces of crucible or slag entrained in the melt during pouring or dirt from a mold that is not cleaned. Indigenous inclusions are from inside the alloy. They form from the molten metal during solidification or subsequent thermo-mechanical processing. For example, it is known that NiTi alloy melted in graphite crucible dissolves carbon from the crucible and precipitate carbides during solidification (Ref 2). Solid state reactions can also form inclusions. Although stoichiometric NiTi is 50 atom percent Ni, most commercial superelastic alloys are Ni-rich and achieve higher mechanical properties and a degree of transformation temperature control by the precipitation of coherent Ti_3Ni_4 during aging at temperatures in the range of 300 to 500 °C. As shown in the binary phase diagram, these alloys can also form the terminal equilibrium phase Ni_3Ti . Depending on chemistry, Ni_3Ti precipitation can occur in times as short as 1 h at 850 °C (Ref 3). There is also the Ti-rich phase,

$Ti_4Ni_2(O,C,N)_x$ first reported by Nishida et al. (Ref 4). This phase is found in Ni-rich alloys. Its presence is caused by microsegregation which increases the Ti, C, N, and O content of the interdendritic regions during solidification (Ref 3).

Through the diligence of the alloy manufacturers, virtually all inclusions in NiTi alloys are indigenous. The type of the inclusions, the amount and the size distribution depend on the raw material used, the melting method and the thermo-mechanical processes used in making the wrought product (Ref 5). In homogeneous products, the indigenous inclusions are uniformly distributed on a macroscopic scale but segregated on a microscopic scale. For alloy melted in graphite, TiC precipitated in the interdendritic regions of the casting, is the primary inclusion species. This causes local variations in matrix Ni/Ti ratio. Other inclusions may be present as described above.

2. Background

In Nitinol for medical products, inclusion content is commonly rated by maximum inclusion size and maximum area fraction pursuant to the ASTM standard (Ref 6). The current requirements of 39 μm and 2.80% maximum were formulated by ASTM Committee F04.12 based on data from SAES Smart Materials. Data on maximum size and maximum area fraction from 104 heats of superelastic alloy with $A_s = -25$ to $+10$ °C manufactured from 1993 to 2000 was analyzed with the assumption of a normal particle size distribution. The 99.99% confidence interval was calculated to set the specification limits.

Vander Voort reviewed methods for inclusion measurement in steels (Ref 7). He observed that rigorous stereological methods are rarely maintained in quantitative metallography. Rather, compromises are made in order to obtain data in a practical amount of time. Alloys designed for fatigue rated applications usually have low inclusion content. Vander Voort also observed that at low inclusion content, the inclusion size range does not have a normal distribution but is skewed. At

This article is an invited paper selected from presentations at the International Conference on Shape Memory and Superelastic Technologies 2011, held November 6-9, 2011, in Hong Kong, China, and has been expanded from the original presentation.

Frank Sczerzenie, Giorgio Vergani, and Clarence Belden, SAES Smart Materials, New Hartford, NY. Contact e-mails: frank_sczerzenie@saes-group.com and giorgio_vergani@saes-group.com.

very low inclusion levels, the issue becomes how to measure and differentiate inclusion content in alloys, in heats or in lots of a product. This paper reports the methodology developed for

NiTi alloys at SAES Smart Materials with the results for various products.

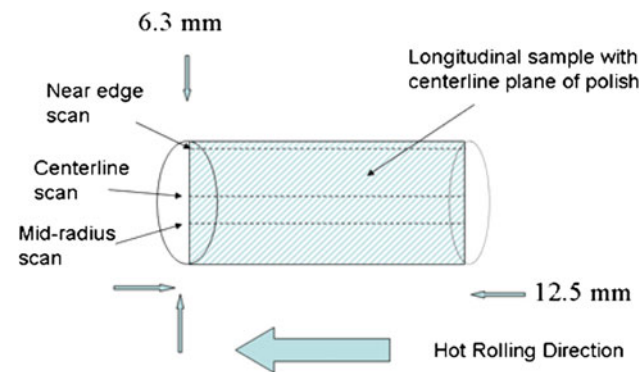


Fig. 1 Schematic of sample from coil and metallographic scanning technique

3. Procedure

The procedures for preparation of coil and wire samples and for the evaluation of maximum inclusion size and maximum area fraction were reported by Sczerzenie et al. at SMST 2010 (Ref 8). Longitudinal centerline samples were polished in stages through 120 grit stone, 240 grit paper, 15 μm diamond, 9 μm diamond, and finally 3 μm diamond. The samples were examined at 500 diameters magnification on a Zeiss Observer D1 M inverted stage metallograph in the as-polished condition. In this condition, carbides intermetallic oxides, voids, and matrix can be differentiated by color in the light microscope. Figure 1 is a schematic of the longitudinal orientation of the metallographic sample in coil and the scanning technique. After scanning, nine fields of view were photographed and analyzed

Table 1 Inclusions in standard and process improvement coil

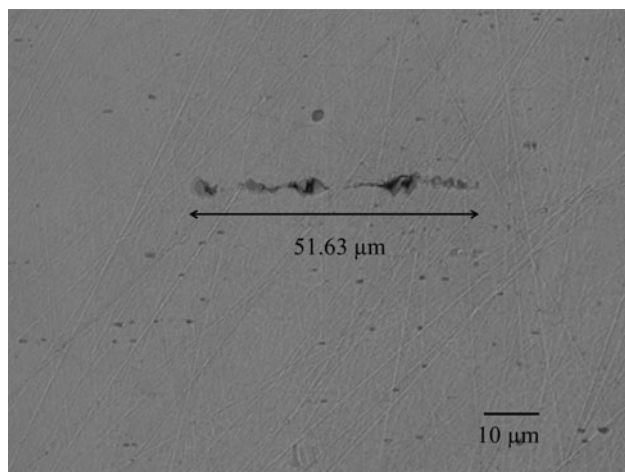
	Standard SE coil	Process improvement coil	Reduction by process improvement
Number of heats	12	3	...
Number of fields	378	198	...
Particles per field	107	95	11.2%
Inclusion average, μm	2.55	2.43	4.7%
Inclusion maximum, μm	25.31	19.23	24.0%
Average area fraction	0.653%	0.493%	24.5%
Maximum area fraction	1.23%	0.91%	26.0%
Carbides per field	102	94	7.8%
Carbide average size, μm	2.5	2.41	3.6%
Carbide maximum, μm	18.15	19.23	-6.0%
Carbide average area fraction	0.488%	0.466%	4.5%
Carbide maximum area fraction	1.06%	0.91%	14.2%
Oxides per field	5	1	80.0%
Oxide average size, μm	5.6	4.85	13.4%
Oxide maximum, μm	25.31	11.95	52.8%
Oxide average area fraction	0.164%	0.026%	84.1%
Oxide maximum area fraction	0.65%	0.19%	70.8%

Table 2 Inclusions in standard and process improvement 2.16 mm diameter wire

	Standard SE wire	Process improvement wire	Reduction by process improvement
Number of heats	12	3	...
Number of fields	108	162	...
Particles per field	151	139	7.9%
Inclusion average, μm	2.26	2.19	3.1%
Maximum inclusion, μm	43.62	27.84	36.2%
Average area fraction	0.68%	0.60%	11.8%
Maximum area fraction	1.45%	1.07%	26.2%
Carbides per field	144	137	4.9%
Carbide average size, μm	2.06	2.13	-3.4%
Carbide maximum, μm	19.94	26.40	-32.4%
Carbide average area fraction	0.49%	0.57%	-16.3%
Carbide maximum area fraction	0.81%	0.97%	-19.8%
Oxides per field	7	2	71.4%
Oxide average size, μm	6.25	5.71	8.6%
Oxide maximum, μm	43.62	27.84	36.2%
Oxide average area fraction	0.19%	0.05%	73.7%
Oxide maximum area fraction	0.91%	0.31%	65.9%

Table 3 Stringers in standard and process improvement 2.16 mm diameter wire

	Standard SE wire	Process improvement wire	Reduction by process improvement
Number of heats	12	3	...
Number of fields	108	162	...
Stringers per field	18.7	17.8	4.8%
Average stringer length, μm	7	7	0.0%
Maximum stringer length, μm	76.36	60.83	20.3%
Average area fraction	0.68%	0.60%	11.8%
Maximum area fraction	1.45%	1.07%	26.2%

**Fig. 2** Stringer in cold drawn wire. C9-8899-7-1

on each sample. For total inclusion measurement, the evaluation method was modified.

Size and area data were compiled for carbides and oxides separately for all particles at or above $0.1\ \mu\text{m}$ in each of the nine fields of view. The data for each species was compiled into a histogram for all inclusions in all fields of view. The maximum dimension for each particle was rounded up to the nearest whole number to construct the histograms. That is any number from 9.01 to $9.99\ \mu\text{m}$ was counted as a $10\text{-}\mu\text{m}$ particle. Area fractions were compiled for each species for all fields of view to develop an area % versus percentile rating. The data in Tables 1, 2 and 3 show the number of fields and number of inclusion particles analyzed for each species in each product form. The histograms show the data normalized by the number of samples in order to show the real change in inclusion species size distribution in each product.

Fracture and separation of particles often created voids between particles in the cold drawn wire. No attempt was made to count void area separately from the oxide or carbide areas. Also, the small diameter and the curved cast of the cold drawn wire did not permit easy scanning of center, mid-radius, and edge regions. Therefore, for cold drawn wires, the entire sample area was scanned and nine fields were photographed to represent the largest particle and/or largest area fraction of inclusions without regard to radial location.

4. Stringer Measurement

An additional challenge was the evaluation of stringers. During the inclusion analyses of wires at diameters smaller than

stipulated by the ASTM F2063, discrepancies were observed between the reported maximum individual inclusion sizes and the length of stringers (Ref 8). An example is shown in Fig. 2. The maximum individual inclusion size for this area is $9.07\ \mu\text{m}$. The large stringer at the top of this field of view is $51.63\ \mu\text{m}$ long.

Prior to this work, individual inclusions were reported separately if they were separated by matrix even though the particles were very closely spaced and their size and shape indicated that the particles had been formed by the break-up of a larger inclusion. Therefore a new methodology was needed to measure stringers.

ASTM E 45-05 Standard test Methods for Determining the Inclusion Content of Steel defines a stringer in Paragraph 3.2.5 as follows:

An individual inclusion that is highly elongated in the deformation direction or three or more Type B [alumina type] or C [silicate type] inclusions aligned in a plane parallel to the hot working axis and off- set by no more than $15\ \mu\text{m}$ with a separation of less than $40\ \mu\text{m}$ between any two nearest neighbor inclusions.

E 45 requires scanning the sample at $100\times$. This is consistent with the structure of the alloys. VIM-VAR NiTi alloy has a higher density of inclusions but a smaller inclusion size than most steels. The ASTM Standard F2063 for NiTi alloys stipulates inclusion evaluation at 400 to $500\times$ in order to resolve the inclusions. Therefore the definition of a stringer used by SAES was modified as follows:

Stringer—an individual inclusion that is highly elongated in the deformation direction or two or more inclusions aligned in a plane parallel to the hot working axis and offset by no more than $1\ \mu\text{m}$ ($0.000039\ \text{in.}$) with separation of less than $5\ \mu\text{m}$ ($0.000195\ \text{in.}$) between any two nearest neighbor inclusions.

The wire samples were re-evaluated for total stringer content pursuant to this definition.

5. Materials and Results

Total inclusion measurement was used to evaluate the effect of process changes aimed at improving microcleanliness in one superelastic alloy formulation that is designated by austenite start temperature, $A_s = -15\ ^\circ\text{C}$. Changes involved modifications to melting and hot working that have not been applied to standard products. Three heats were processed to $6.3\ \text{mm}$ diameter hot rolled coil and $2.16\ \text{mm}$ diameter cold drawn wire and compared to standard product that were the same alloy formulation. For the standard products, the most recent 12 heats

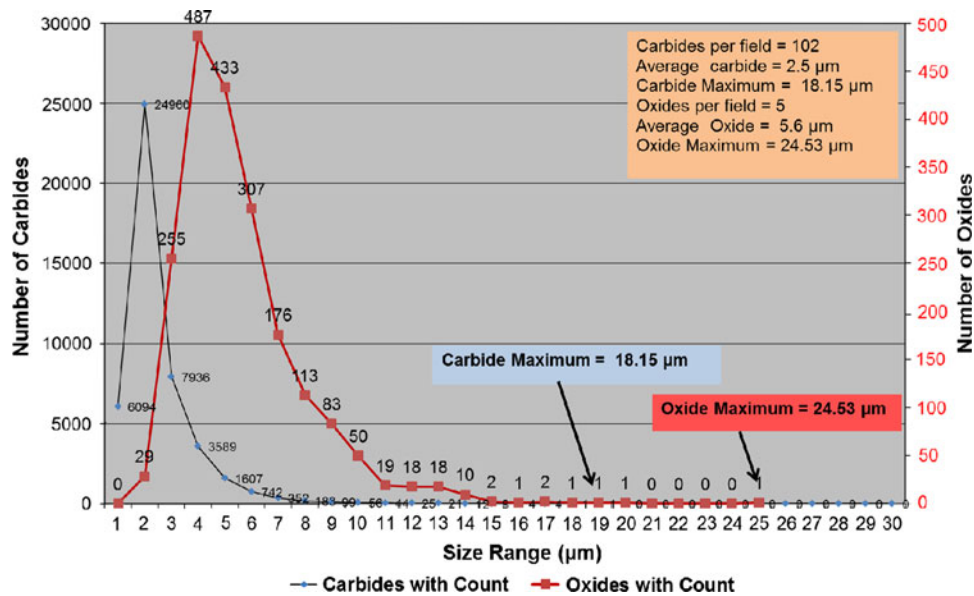


Fig. 3 Standard process coil carbide and oxide size distributions normalized by the number of samples

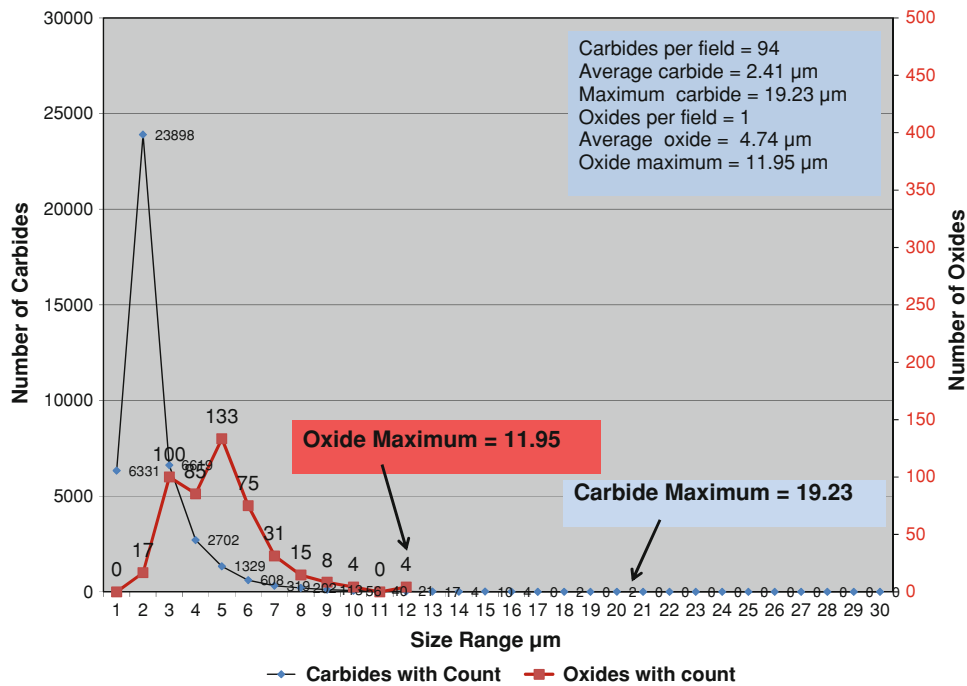


Fig. 4 Process improvement coil, carbide, and oxide size distribution normalized by the number of samples

of product finished to coil and wire were evaluated. In order to evaluate the effect of the changes with data from a different number of heats, the data was normalized by the number of samples in the standard and in the process change groups, respectively.

the size and area fraction of intermetallic oxides. The number and area fraction of carbides is decreased slightly. Maximum carbide size is increased slightly. Maximum area fraction and maximum inclusion size were reduced by 26 and 24%, respectively.

6. Hot Rolled Coil

Table 1 and Fig. 3-6 compare inclusion populations in standard and improved coil. The data shows a large reduction in

7. Cold Drawn Wire

Table 2 and Fig. 7-10 compare inclusion populations in standard and improved process cold drawn wire. Maximum

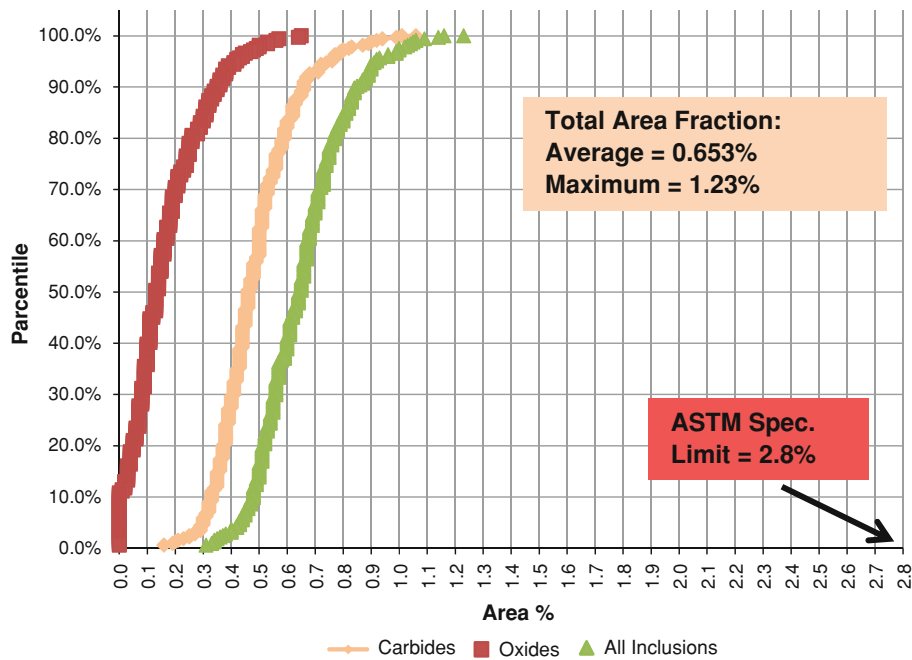


Fig. 5 Standard process coil, percentile vs. area fraction of carbides, oxides, and all inclusions

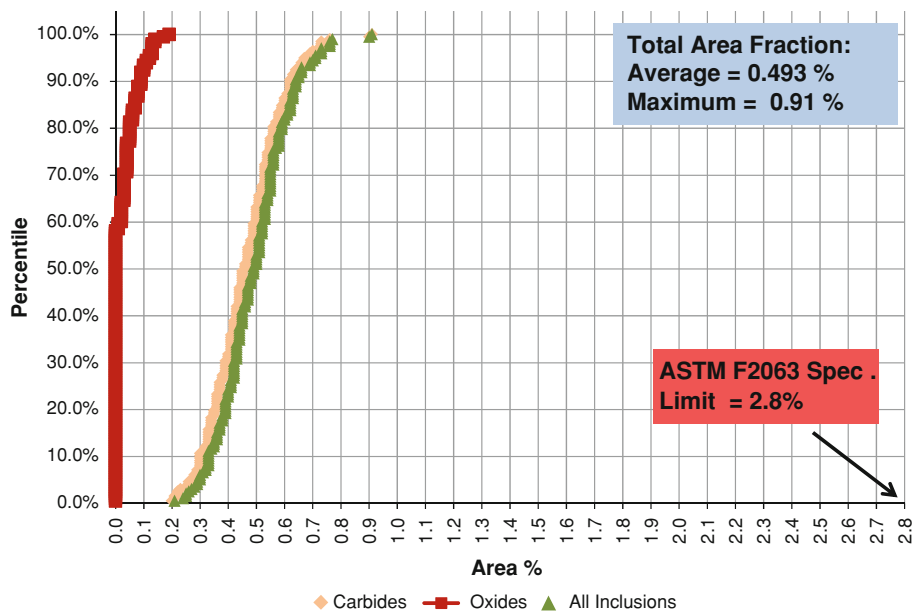


Fig. 6 Process improvement coil, percentile vs. area fraction of carbides, oxides and all inclusions

area fraction and maximum inclusion size were reduced by 26 and 36%, respectively. This is consistent with the changes measured in the hot rolled coil.

7.1 Stringers

Stringers were measured in the cold drawn wire. Table 3 and Fig. 11 show that maximum stringer length is reduced from 76.36 to 60.83 μm by the improved process. The number of stringers per field is reduced by 4.8%. The maximum length of

stringers is reduced 20% and the maximum area for stringers is reduced 26% by the improved process.

8. Discussion

This work has demonstrated a method to analyze the total inclusion content of NiTi alloys. Pursuant to ASTM Standards,

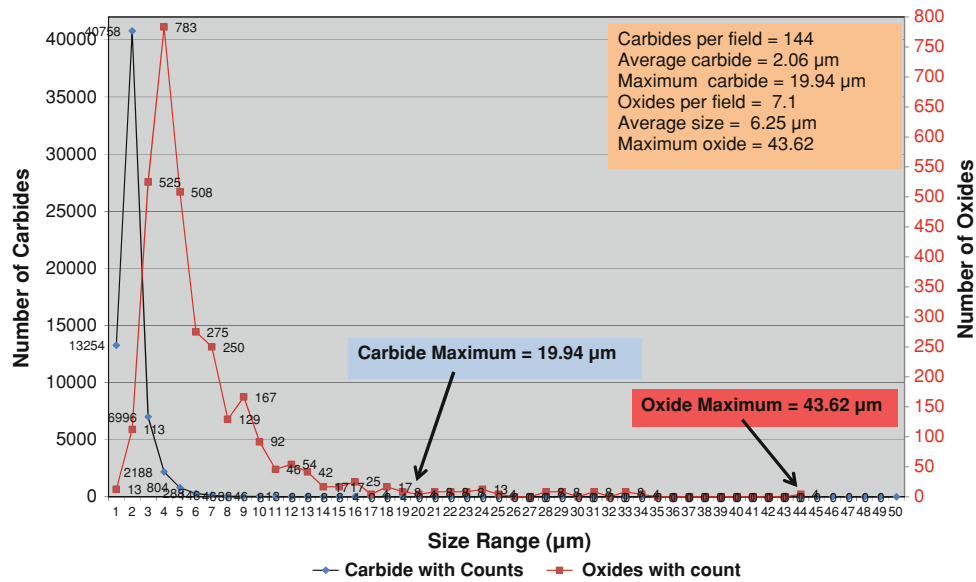


Fig. 7 Standard process redraw wire, carbide and oxide size distributions normalized by the number of samples

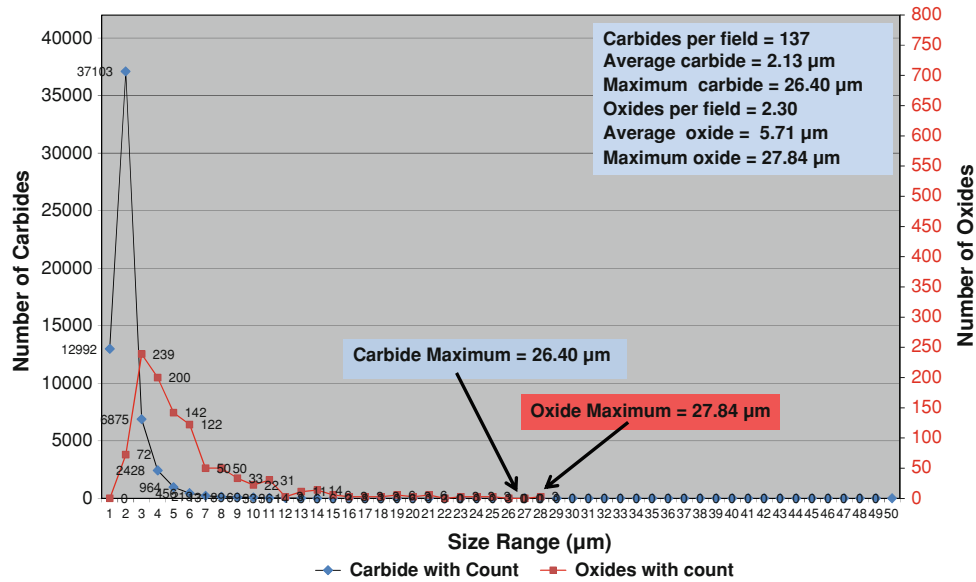


Fig. 8 Process improvement redraw wire, carbide and oxide size distributions normalized by the number of samples

a definition for stringers has been formulated and applied to cold drawn wire.

The particle size distributions of both carbides and oxides are not normal in both standard and improved process materials. These distributions are skewed toward positive values with relatively few larger particles approaching the maximum particle size. To quantify this, normality tests were done in the Minitab™ statistical analysis program. For example, *p* values are much less than 0.05 in the Anderson Darling Normality test as shown for carbides in standard product, Fig. 12.

The histograms for particle size distribution were compared to several statistical distribution curves in Minitab™. As shown

in Fig. 13 for carbides in standard coil, the Weibull model was the best fit to the data. However the maximum of the Weibull model is at 9 μm versus the coil maximum at 18.15 μm. Similar differences were obtained for oxides in coil and for carbides and oxides in improved process coil. Hence, more work needs to be done to calculate a maximum predicted inclusion size.

Toro reported that cold drawing increases stringer formation in superelastic tubing (Ref 9). He attributed stringer formation to the break-up of oxides. Comparing stringers in standard wire to stringers in improved process wire shows that even though oxide density and area fraction were reduced by over 70%, the density and average area fraction of stringers was reduced by

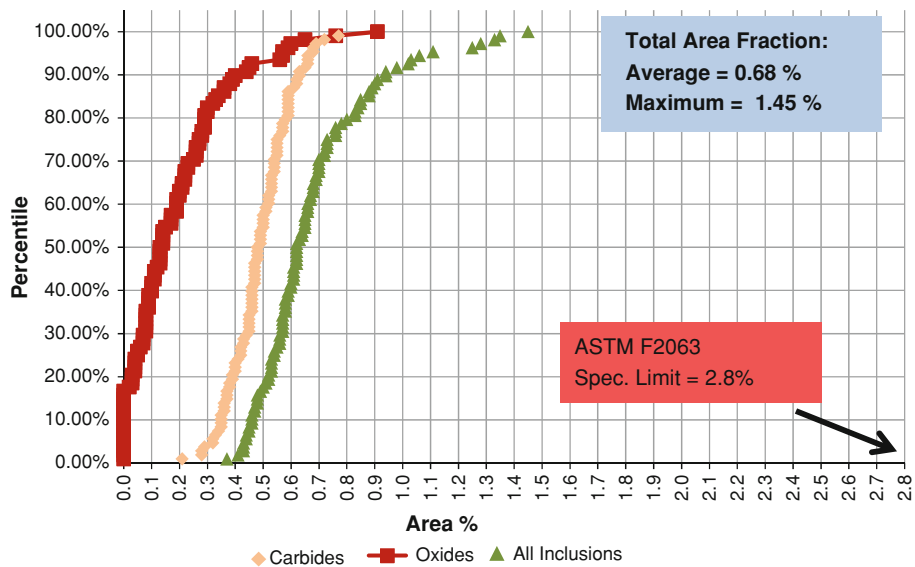


Fig. 9 Standard process redraw wire, percentile vs. area fraction of carbides, oxides, and all inclusions

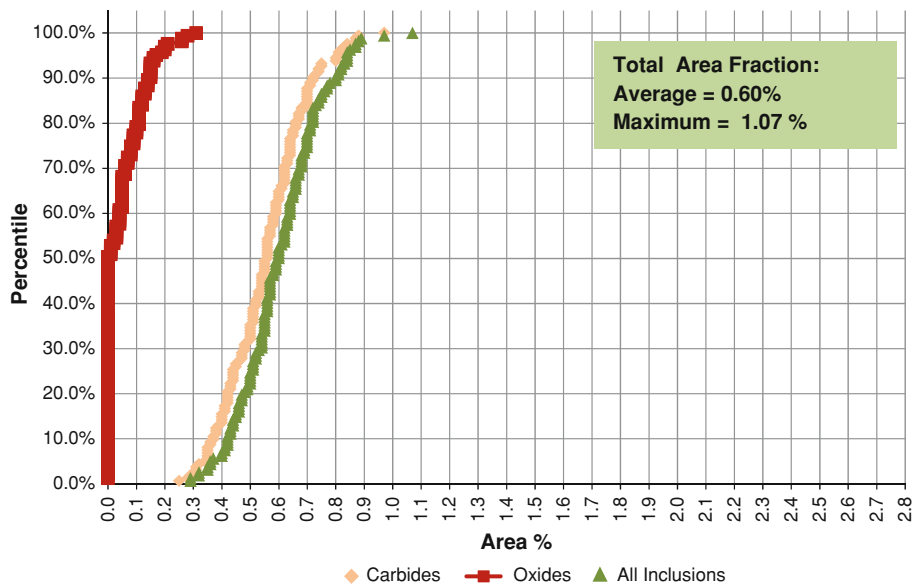


Fig. 10 Process improvement redraw wire, percentile vs. area fraction of carbides, oxides, and all inclusions

only 4.8 and 11.8%, respectively. Maximum stringer length was reduced by 20%. This demonstrates that both carbides and oxides form stringers in VIM-VAR superelastic wire. In cold drawing, area fraction is increased by the fracture of inclusions and the formation of voids between particles. Separation of inclusions from the matrix and the formation of voids in the drawing direction in front and behind inclusions also increases area fraction. The overall reduction in maximum size and area fraction of inclusions in improved process coil was the result of reducing the number, size and area fraction of intermetallic oxides. While the density, average size, and the area fraction of carbides decreased slightly, the maximum carbide size increased by the improved process. The reasons for this require

a further investigation. Subsequently, in the cold drawn wire, the number of carbides per field was reduced slightly and the average size, maximum size, and area fraction of carbides increased. Since the average size of carbides was decreased in coil by the improved process, this indicates that the finer carbides are less likely to break-up in cold drawing.

9. Conclusions

Inclusion size distributions have been measured in a superelastic formulation of NiTi alloy in hot rolled coil and

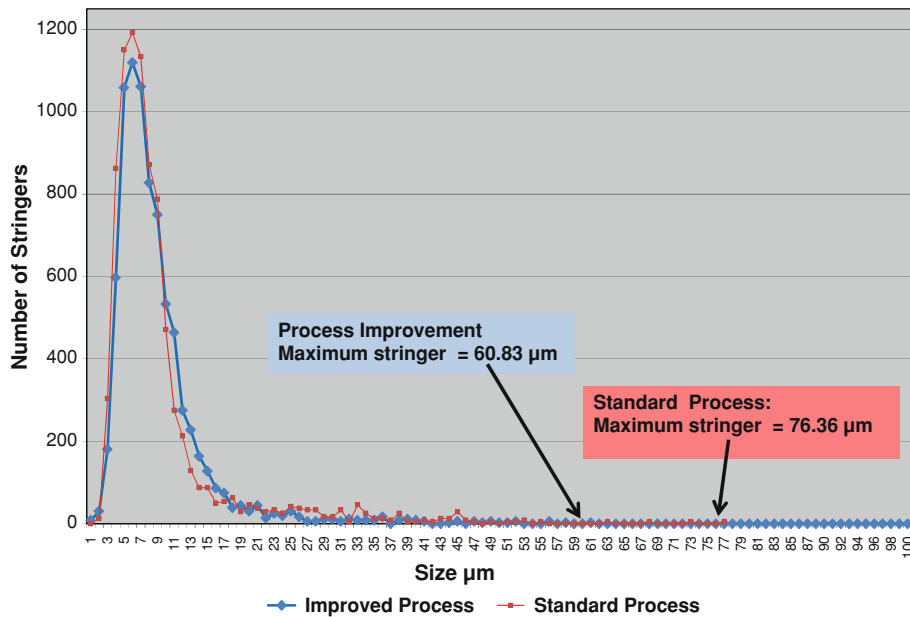


Fig. 11 Stringer size distribution, standard vs. process improvement normalized by the number of samples

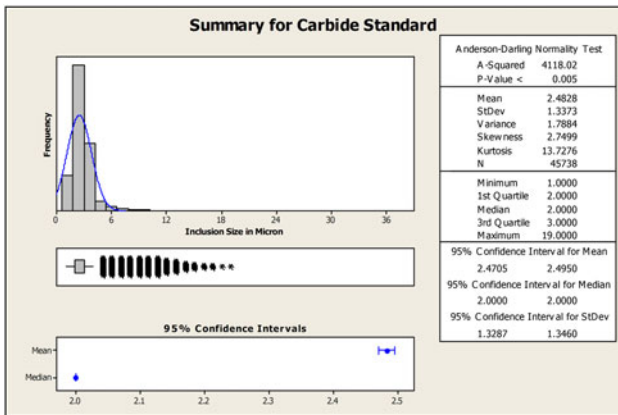


Fig. 12 Anderson Darling Normality test of carbide distribution in standard process coil

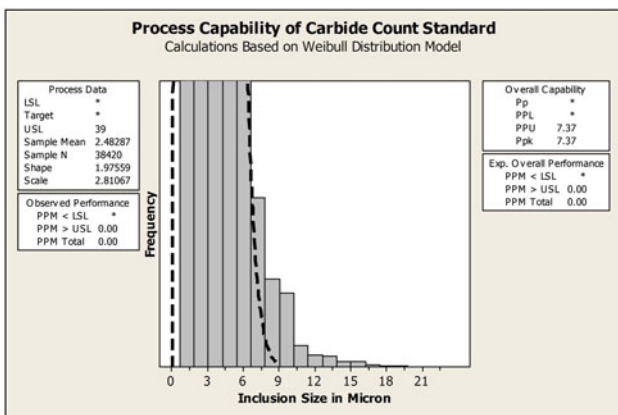


Fig. 13 Weibull curve for the carbide size distribution in standard coil

cold drawn wires. The numerical data cannot be used for all NiTi alloys because changing NiTi ratio results in changes in the relative amount and size of carbides and intermetallic oxide inclusions (Ref 8). However, similar distributions have been observed in other VIM-VAR superelastic alloy formulations and product forms such as small diameter bar. Similar distributions are also found in superelastic alloy made by other melting methods.

This methodology for total inclusion measurement has been applied to the evaluation of process changes. The data demonstrates that process change can result in reductions in maximum inclusion size and area fraction in hot worked product. This results in a reduction in inclusion size and area fraction in subsequent cold drawing and a reduction in maximum stringer length.

This work has demonstrated that the inclusion size distributions in superelastic VIM-VAR NiTi alloy are not normal. They are positively skewed with a few particles near the maximum observed size. The use of the statistics of normal distributions with a six sigma confidence interval or the use of non-normal distributions such as Weibull analysis to calculate the maximum value for inclusion size is not valid for these alloys. Therefore, defining inclusion size and area fraction limits becomes a matter of applying Extreme Value Statistics in future work (Ref 10, 11).

For the alloy formulation evaluated in this work, all hot rolled coils had maximum inclusion size below 25.5 µm and area fractions of inclusions below 1.5%. Similar maxima were observed in precursor bar for tubing. These maxima are significantly below the current ASTM Standard limits.

References

1. D. Bradley et al., Optimization of Melt Chemistry and Properties of 35Cobalt-35Nickel-20Chromium-10Molybdenum Alloy Medical Grade Wire, *Conference on Materials and Processes for Medical Devices*, ASM International, Anaheim, CA, Sept 8, 2003, p 1–7

2. J. Frenzel et al., Influence of Carbon on Martensitic Phase Transformations in NiTi Shape Memory Alloys, *Acta Mater.*, 2007, **55**, p 1331–1341
3. V.N. Khodorenko et al., Effect of the Composition of a Titanium Nickelide Alloy on Its Structure and on the Formation of the Grain Boundary Ensemble, *Russ. Phys. J.*, 2011, **53**(8), p 827–834
4. M. Nishida, C.M. Wayman, and T. Honma, Precipitation Processes in Near-Equiatomic TiNi Shape Memory Alloys, *Metall. Trans. A*, 1986, **17**, p 1505–1515
5. N. Morgan et al., Carbon and Oxygen Levels in Nitinol Alloys and the Implications for Medical Device Manufacture and Durability, *Proceedings of the International Conference on Shape Memory and Superelastic Technologies*, B. Berg et al., Ed., ASM International, 2006, p 821–828
6. F 2063-05, Standard Specification for Wrought Nickel-Titanium Shape Memory Alloys for Medical Devices and Surgical Implants, ASTM International, West Conshohocken, PA
7. G. Vander Voort, Inclusion Measurement, *Metallography as a Quality Control Tool*, J. McCall and P.M. French, Ed., Plenum Press, New York, 1979, p 1–88
8. F. Sczerzenie et al., Comparison of Inclusions in Cold Drawn Wire and Precursor Hot-Rolled Rod Coil in VIM-VAR Nickel-Titanium Alloy, *J. Mater. Eng. Perform.*, 2011, **20**(4–5), p 752–756
9. A. Toro et al., Characterization of Non-Metallic Inclusions in Superelastic NiTi Tubes, *J. Mater. Eng. Perform.*, 2009, **18**(5–6), p 448–458
10. S. Beretta and C.W. Anderson, Extreme Value Statistics in Metal Fatigue, Societ'a Italiana di Statistica, Atti della XLI Riunione Scientifica, 2002, p 251–260
11. E 2283 Standard Practice for Extreme Value Analysis of Nonmetallic Inclusions in Steel and Other Microstructural Features, ASTM International, West Conshohocken, PA